Energy Reports 14 (2025) 3118–3131

Contents lists available at ScienceDirect

Energy Reports

journal homepage: www.elsevier.com/locate/egyr

Research Paper

Can digital twin technology revolutionize wildfire management and energy resilience in Los Angeles?☆

Mohannad Alhazmi [a], Olivia Peijin Li [b], Da Huo [c,*], Hanjin Zhang [d], Zhaoyao Bao [e]

[a] Electrical Engineering Department, College of Applied Engineering, King Saud University, Riyadh, Saudi Arabia
[b] College of Mechanical Engineering, Taiyuan University of Technology, Taiyuan, China
[c] School of Water, Energy and Environment, Cranfield University, Bedford, UK
[d] School of Software & Internet of Things Engineering, Jiangxi University of Finance and Economics, Nanchang, China
[e] Civil and Environmental Engineering , Cornell University, Ithaca, NY, USA

ARTICLE INFO

Keywords:
Wildfires
Digital twin
Distributionally robust optimization
Microgrid resilience
Energy-water nexus
Wildfire dynamics
Resource allocation optimization

ABSTRACT

Wildfires increasingly threaten energy and water infrastructure in regions such as Los Angeles (LA), requiring real-time, resilient coordination strategies. This study introduces an integrated framework that combines digital twin technology with distributionally robust optimization (DRO) to manage uncertainty and improve operational resilience. The system dynamically models wildfire spread using terrain and wind data, and jointly simulates energy and water systems under real-time disruption scenarios. Validation is performed using real-world data from the Palisades Fire, benchmarked against deterministic dispatch models without robust adaptation. Simulation results show that the DRO-based method reduces average PV efficiency loss by 22.4% through real-time reconfiguration and increases battery discharge support during evacuation surges by 18.7%. Compared to baseline strategies, the proposed framework shortens average critical load outage duration by 35%, improves firefighting water delivery reliability by 21.8%, and lowers total daily water consumption by 12.5 million gallons. Fire spread prediction achieves a 24-hour localization error below 310 meters, ensuring precise hazard mapping. These outcomes confirm the framework's ability to enhance system resilience, minimize resource waste, and support post-disaster recovery. The presented approach offers a scalable and adaptive tool for next-generation wildfire response planning under complex, uncertain conditions.

1. Introduction

As of January 2025, Los Angeles (LA) is experiencing one of the most severe wildfire disasters in its recent history. The Palisades Fire, which ignited on January 7, has burned over 24,000 acres, destroyed more than 12,300 structures, and forced the evacuation of approximately 200,000 residents (Ermagun et al., 2025; Analytica, 2025). The disaster has tragically led to 27 confirmed fatalities, with dozens still unaccounted for. This extreme event results from a confluence of environmental stressors, including prolonged drought, high vegetation density, and wind gusts exceeding 100 mph in elevated terrain—factors that collectively render containment efforts exceedingly difficult. The magnitude of the crisis underscores the urgent demand for advanced tools capable of mitigating wildfire impacts and enhancing urban resilience (Youvan, 2025). The current situation has revealed significant weaknesses in LA's infrastructure systems, especially within the energy sector. Microgrids have been recognized as a promising solution for maintaining energy availability during central grid disruptions (Zhao et al., 2024a), and their integration with renewable sources enables decentralized energy control under hazardous conditions (Solat et al., 2024). However, under fast-evolving wildfire threats, conventional microgrid systems often lack the adaptability required to respond in real time (Xiao et al., 2024). Certain approaches have explored dynamic microgrid configurations and islanding control, though challenges remain in maintaining system stability during extreme events (Gao et al., 2023). In the case of the Palisades Fire, widespread power interruptions have been reported due to transmission line damage and wildfire-induced smoke, which has reduced photovoltaic (PV) efficiency by as much as 50% in affected regions (Gao and Ai, 2024). These energy challenges are further complicated by interdependent water infrastructure systems, which are simultaneously burdened by heightened firefighting demand and constrained supply availability. This reveals the critical need for integrated and adaptive wildfire management frameworks that

☆ This article is part of a Special issue entitled: 'VSI: AI-enabled Power Systems(Haixin Wang)' published in Energy Reports.

* Corresponding author.
E-mail address: Da.Huo@cranfield.ac.uk (D. Huo).

https://doi.org/10.1016/j.egyr.2025.09.008
Received 7 June 2025; Received in revised form 29 July 2025; Accepted 19 September 2025
Available online 15 October 2025
2352-4847/© 2025 The Authors. Published by Elsevier Ltd. This is an open access article under the CC BY license (http://creativecommons.org/licenses/by/4.0/).

jointly consider the dynamics of power distribution, water resources, and environmental hazards.

In response to these challenges, this paper introduces a novel framework that integrates digital twin technology with advanced optimization models to address the complexities of wildfire management. Digital twins, virtual representations of physical assets, provide a dynamic platform for real-time monitoring, simulation, and decision-making. By leveraging real-time data on fire spread, weather conditions, and infrastructure status, digital twins enable proactive resource allocation and operational strategies. In this study, the digital twin platform is enhanced with distributionally robust optimization (DRO) to manage the uncertainties inherent in wildfire scenarios, such as stochastic renewable energy generation, variable water availability, and unpredictable fire behavior. A key innovation of this research lies in its incorporation of detailed wildfire dynamics into the optimization framework. Unlike existing approaches that treat wildfires as static or simplified phenomena, this study employs advanced fire spread models that account for wind speed, topography, vegetation density, and real-time suppression actions. The framework also includes post-fire recovery models to ensure efficient allocation of resources for infrastructure repair and community restoration. These capabilities are validated through case studies based on real-time data from the ongoing Palisades Fire, demonstrating the framework's ability to enhance resilience and optimize resource use under extreme conditions. This research contributes to bridging the gap between wildfire management and energy system resilience by providing a holistic approach that integrates both domains. While previous studies have primarily focused on isolated aspects of wildfire mitigation or energy system optimization, this paper emphasizes their interdependencies. The integration of digital twin technology with DRO advances the state of the art in adaptive disaster management and offers practical solutions tailored to the unique challenges of wildfire-prone regions like Los Angeles. The contributions of this paper are summarized as follows:

1. Development of a Digital Twin-Based Framework for Wildfire Management: This study introduces a comprehensive digital twin platform that integrates energy systems, water resources, and wildfire dynamics. The platform supports real-time simulations and predictive analytics, empowering decision-makers with actionable insights during wildfire events.

2. Integration of Advanced Wildfire Dynamics into Optimization Models: The research incorporates detailed fire spread models that include factors such as wind, topography, and vegetation. This dynamic modeling capability enhances the accuracy and reliability of resource allocation and resilience strategies.

3. Application of Distributionally Robust Optimization for Uncertainty Management: By leveraging DRO, the framework effectively addresses the uncertainties inherent in wildfire scenarios, enabling robust and adaptive decision-making under extreme conditions.

4. Validation Through Real-Time Case Studies: The methodology is validated using data from the ongoing LA wildfires, including the Palisades Fire. These case studies demonstrate the framework's effectiveness in minimizing disruptions, optimizing resource allocation, and supporting post-fire recovery efforts.

2. Literature review

Wildfire modeling has evolved significantly, transitioning from early empirical formulations to advanced simulation platforms. One foundational approach introduced in the 1970s established a method for estimating surface fire spread based on fuel type, wind conditions, and terrain slope (Scott, 2005). Building upon this, subsequent models enabled spatial and temporal fire growth simulation through the integration of geospatial inputs and environmental variability (Price and Germino, 2022; Ghodrat et al., 2022). Further advancements introduced software-based frameworks capable of dynamically capturing fire–wind interactions, improving adaptability to real-time conditions (Jain et al., 2022). The influence of wind speed and direction has been identified as a dominant factor in fire propagation, especially in regions prone to rapid directional changes during wildfire events (Swann et al., 2024). In parallel, research has shown that vegetation density and composition are critical to determining fire intensity and severity, reinforcing the necessity of localized fuel management strategies (Brody-Heine et al., 2023; Li et al., 2025a). Metrics incorporating wind vector dynamics have also been proposed to refine fire risk evaluation and enhance situational awareness in mountainous and coastal terrains (Rahiminejad et al., 2023). While these models represent major technical progress, most remain focused solely on fire behavior, overlooking the bidirectional interactions between wildfire evolution and the performance of critical infrastructure systems such as energy and water networks.

The increasing frequency and severity of wildfires have spurred substantial research aimed at enhancing the resilience of energy systems, particularly in fire-prone urban and peri-urban regions. Among various strategies, microgrids have gained prominence due to their capacity for autonomous operation during main grid outages (Umunnakwe et al., 2021; Zhao et al., 2024b). Their modularity and ability to support localized energy provision make them well-suited for hazard-adaptive applications. Efforts have also been made to integrate renewable energy sources, such as photovoltaic (PV) systems and battery storage, into microgrid configurations to improve sustainability and operational independence during emergencies (Dobrinkova, 2024). To strengthen performance under uncertain conditions, advanced control methods have been developed to enable real-time switching, adaptive protection, and decentralized load management (Abdelmalak and Benidris, 2022). Nonetheless, many existing microgrid designs remain constrained by static configurations, which often fail to respond effectively to rapidly evolving fire spread and infrastructure risk (Zhao et al., 2025; Cui et al., 2024). In addition, the interdependence between energy and other critical systems — particularly water infrastructure — remains insufficiently addressed in wildfire scenarios. As firefighting efforts escalate, energy systems are expected to continue powering essential services, while water demands surge simultaneously. PV-based microgrids, however, are highly sensitive to smoke and heat stress during wildfires. Studies have shown that suspended particulate matter can reduce solar generation efficiency by 30%–50% in affected regions (Bassey et al., 2024). Other investigations indicate that spectral distortion and thermal overload may cause inverter instability or shutdowns, threatening power continuity during critical response periods (Cao and Zhou, 2024; Li et al., 2025b). Without adaptive planning and integrated control, these disruptions risk amplifying systemic vulnerabilities and undermining emergency response capability.

In parallel, digital twin technology has gained increasing traction as a next-generation tool for real-time system modeling, asset tracking, and scenario forecasting. In the context of disaster management, digital twins offer a virtualized layer for monitoring infrastructure conditions, simulating environmental hazards, and deploying adaptive control strategies under uncertainty (Boakye-Boateng et al., 2025). These platforms replicate physical assets in a cyber–physical environment, continuously updated through sensor data streams, historical records, and predictive algorithms. Their application in industrial systems has been demonstrated in areas such as fault diagnostics, failure prediction, and supply chain disruption management (Yu and He, 2022). When applied to energy systems, digital twins enable operators to visualize grid status, anticipate cascading failures, and execute preventative maintenance schedules. However, their deployment in wildfire-prone environments is still in the early stages of development. Many existing implementations focus narrowly on modeling infrastructure exposure or simulating generic fire perimeters, without capturing the dynamic co-evolution of wildfire behavior, resource availability, and infrastructure response. Recent studies have begun integrating digital twins with renewable energy control and smart grid optimization modules, emphasizing the need for real-time environmental feedback, scalable computing, and adaptive learning capabilities (Zhao et al., 2024c).

Table 1
Nomenclature table for key decision and state variables.

Symbol	Description	Unit
$\Phi_{i,t}$	Power generation at node i and time t	kW
$\Psi_{i,t}$	Water usage at node i and time t	m^3
$\Sigma_{i,t}$	Firefighting cost at node i and time t	$
$\mathscr{F}_{k,t}$	Energy flow on line k at time t	kW
$\chi_{k,t}$	Emission from line k at time t	kg CO_2
$\Theta_{j,t}$	Infrastructure damage state at node j, time t	–
$\kappa_{j,t}$	Resilience degradation coefficient	–
$\rho_{m,t}$	Resource scarcity at sector m, time t	–
$\pi_{m,t}^{\text{damage}}$	Environmental damage at sector m, time t	–
$\Xi_{n,t}$	Critical infrastructure status at node n, time t	–
$\Omega_{n,t}$	Resource loss at critical node n, time t	kWh or m^3
$P_{n,t}^{\text{gen}}$	Power generation at node n, time t	kW
$P_{n,t}^{\text{store}}$	Power from storage at node n, time t	kW
$P_{n,t}^{\text{demand}}$	Power demand at node n, time t	kW
$W_{m,t}^{\text{avail}}$	Available water at resource m, time t	m^3
$W_{m,t}^{\text{essential}}$	Essential water need at m, time t	m^3
$P_{n,t}^{\text{PV}}$	PV power generation at node n, time t	kW
$\eta_{n,t}^{\text{PV}}$	PV efficiency at node n, time t	%
$\sigma_{n,t}^{\text{smoke}}$	Smoke-induced efficiency loss at node n, t	%
$T_{e,t}$	Temperature of component e at time t	°C
T^{ref}	Reference operating temperature	°C

While preliminary attempts have been made to apply these techniques to disaster response applications, comprehensive solutions that bridge fire dynamics, energy dispatch, and water resource coordination remain an open challenge.

3. Mathematical formulation

The mathematical modeling framework developed in this study addresses the critical need for an adaptive and integrated approach to wildfire management, with a particular emphasis on enhancing energy system resilience, optimizing water resource allocation, and safeguarding critical infrastructure. Wildfires are characterized by rapid propagation, uncertain dynamics, and complex interdependencies between natural and human-engineered systems. To fully capture this complexity, the proposed framework introduces a robust multi-objective optimization model that dynamically links wildfire spread behavior, distributed energy operations, and firefighting water usage. This formulation leverages DRO to accommodate scenario-based uncertainty in renewable generation, resource availability, and fire progression patterns. All control-related parameters involved in the simulation — including load prioritization weights, PV derating factors, water allocation ratios, and dispatch penalties — were selected based on a combination of literature-informed benchmarks, regional operational standards, and preliminary sensitivity analysis. These values were iteratively refined to ensure solution stability and realistic system responses under stress conditions, without relying on full-scale parameter optimization. In parallel, dynamic wildfire modeling components were informed by real-world terrain data, wind conditions, and fuel density, ensuring high-fidelity representation of fire growth across heterogeneous landscapes. Constraints related to energy supply–demand balance, water withdrawal limits, infrastructure reliability, and emergency load coverage were rigorously formulated to ensure operational feasibility and interpretability. The integrated optimization thus enables spatially and temporally adaptive decision-making under disaster conditions, supporting resilient microgrid operation and prioritized water allocation. Overall, the proposed model provides a comprehensive mathematical foundation for managing wildfire-induced disruptions and enhancing critical infrastructure resilience in vulnerable regions.

To ensure clarity in the mathematical formulation, all variables and parameters used in this study are defined in the following nomenclature table (see Tables 1 and 3).

$$\min_{\Phi,\,\Psi,\,\Sigma} \sum_{t=1}^{T} \sum_{i\in\mathscr{N}} \left(\alpha_{i,t}^{\text{gen}} \cdot \Phi_{i,t} + \beta_{i,t}^{\text{water}} \cdot \Psi_{i,t} + \gamma_{i,t}^{\text{fire}} \cdot \Sigma_{i,t} \right) + \sum_{k\in\mathscr{L}} \left(\omega_k^{\text{line}} \cdot \lambda_k \cdot \mathscr{F}_{k,t} + \delta^{\text{emission}} \cdot \chi_{k,t} \right) \tag{1}$$

This equation minimizes the total operational cost, including costs for energy generation ($\alpha_{i,t}^{\text{gen}}$), water distribution ($\beta_{i,t}^{\text{water}}$), and firefighting activities ($\gamma_{i,t}^{\text{fire}}$). The second term considers wildfire-related line losses (ω_k^{line}) and emissions ($\delta^{\text{emission}} \cdot \chi_{k,t}$), summed over all grid nodes i, time periods t, and transmission lines k.

$$\min_{\Theta} \sum_{t=1}^{T} \left(\sum_{j\in\mathscr{F}} \left(\mu_{j,t}^{\text{infra}} \cdot \Theta_{j,t} + \nu_{j,t}^{\text{res}} \cdot \left(\frac{1}{1+e^{-\kappa_{j,t}}} \right) \right) \right) + \sum_{m\in\mathscr{M}} \left(\zeta_{m,t}^{\text{scarcity}} \cdot \rho_{m,t} + \eta^{\text{env}} \cdot \pi_{m,t}^{\text{damage}} \right) \tag{2}$$

This equation minimizes wildfire-related resilience costs, incorporating infrastructure damage costs ($\mu_{j,t}^{\text{infra}} \cdot \Theta_{j,t}$), resilience degradation ($\nu_{j,t}^{\text{res}} \cdot \frac{1}{1+e^{-\kappa_{j,t}}}$), resource scarcity penalties ($\zeta_{m,t}^{\text{scarcity}} \cdot \rho_{m,t}$), and environmental damage ($\eta^{\text{env}} \cdot \pi_{m,t}^{\text{damage}}$) across all impacted nodes j and sectors m.

$$\max_{\Xi} \sum_{t=1}^{T} \sum_{n\in\mathscr{C}} \left(\sigma_{n,t}^{\text{crit}} \cdot \Xi_{n,t} - \varphi_{n,t}^{\text{loss}} \cdot \Omega_{n,t} \right) \tag{3}$$

This equation maximizes microgrid resilience by prioritizing critical infrastructure availability ($\sigma_{n,t}^{\text{crit}} \cdot \Xi_{n,t}$) while penalizing resource loss ($\varphi_{n,t}^{\text{loss}} \cdot \Omega_{n,t}$). It ensures essential operations during wildfires by focusing on nodes n classified as critical ($\mathscr{C}$).

$$\min_{\Lambda} \left(\omega^{\text{cost}} \cdot \sum_{i\in\mathscr{N}} \Phi_{i,t} + \omega^{\text{resilience}} \cdot \sum_{j\in\mathscr{F}} \Theta_{j,t} \right) \tag{4}$$

This multi-objective trade-off optimization balances operational costs ($\Phi_{i,t}$) with resilience improvements ($\Theta_{j,t}$) using weighted factors ω^{cost} and $\omega^{\text{resilience}}$. By tuning these weights, decision-makers can align strategies with cost-effectiveness or resilience priorities.

$$\sum_{n\in\mathscr{N}} \left(P_{n,t}^{\text{gen}} + P_{n,t}^{\text{store}} + \sum_{k\in\mathscr{K}} \mathscr{F}_{k,t}^{\text{in}} \right) = \sum_{n\in\mathscr{N}} \left(P_{n,t}^{\text{demand}} + P_{n,t}^{\text{loss}} + \sum_{k\in\mathscr{K}} \mathscr{F}_{k,t}^{\text{out}} \right), \tag{5}$$

This constraint ensures energy balance, where the total energy supplied (generation, storage, and incoming flow) equals the total energy consumed (demand, losses, and outgoing flow) at every node n and time t. It integrates energy transfer between nodes via flows $\mathscr{F}_{k,t}$ for transmission lines k.

$$\sum_{m\in\mathscr{M}} \left(W_{m,t}^{\text{avail}} - W_{m,t}^{\text{fire}} \right) \geq \sum_{m\in\mathscr{M}} \left(W_{m,t}^{\text{essential}} + W_{m,t}^{\text{loss}} \right), \tag{6}$$

This constraint enforces water balance, ensuring sufficient availability ($W_{m,t}^{\text{avail}}$) for essential needs ($W_{m,t}^{\text{essential}}$) and firefighting ($W_{m,t}^{\text{fire}}$) while accounting for water losses ($W_{m,t}^{\text{loss}}$) at each resource site m.

$$P_{n,t}^{\text{PV}} = \eta_{n,t}^{\text{PV}} \cdot A_{n,t}^{\text{PV}} \cdot \left(1 - \sigma_{n,t}^{\text{smoke}} \right), \tag{7}$$

This equation models renewable energy degradation due to wildfires. The photovoltaic (PV) power generated ($P_{n,t}^{\text{PV}}$) depends on efficiency ($\eta_{n,t}^{\text{PV}}$), panel area ($A_{n,t}^{\text{PV}}$), and smoke-related efficiency loss ($\sigma_{n,t}^{\text{smoke}}$). It dynamically adjusts generation based on wildfire impacts.

$$\eta_{e,t}^{\text{store}} = \eta_e^{\text{base}} \cdot \left(1 - \phi_{e,t}^{\text{temp}} \cdot \left(T_{e,t} - T^{\text{ref}} \right)^2 \right) \tag{8}$$

This equation defines the operational efficiency $\eta_{e,t}^{\text{store}}$ of energy storage system e during time t, accounting for the base efficiency η_e^{base} and temperature-induced efficiency reductions. The term $\phi_{e,t}^{\text{temp}} \cdot \left(T_{e,t} - T^{\text{ref}} \right)^2$ models the quadratic dependency of efficiency losses on the deviation of storage system temperature $T_{e,t}$ from the reference temperature T^{ref}.

$$\frac{\partial A_f(x,y,t)}{\partial t} = v_f(x,y,t) \cdot \left(\alpha_f^{\text{wind}} \cdot W_f(x,y,t) + \alpha_f^{\text{fuel}} \cdot \Lambda_f(x,y) \right) \tag{9}$$

This equation models the wildfire growth over area $A_f(x,y,t)$ as a function of time t, incorporating the fire spread velocity $v_f(x,y,t)$. The velocity depends on wind speed $W_f(x,y,t)$, vegetation density $\Lambda_f(x,y)$, and their respective influence factors α_f^{wind} and α_f^{fuel}.

$$\Delta x_{f,t} = \frac{1}{\beta_f} \cdot \left(\cos(\theta_{f,t}) \cdot v_{f,t}^{\text{wind}} + \sin(\theta_{f,t}) \cdot v_{f,t}^{\text{topo}} \right) \tag{10}$$

This equation captures the spatial propagation of wildfire in the x-direction ($\Delta x_{f,t}$) during time t, considering wind-driven spread ($v_{f,t}^{\text{wind}}$) and topography-driven effects ($v_{f,t}^{\text{topo}}$), weighted by directional factors $\cos(\theta_{f,t})$ and $\sin(\theta_{f,t})$.

$$\Delta A_{f,t} = \int_0^t \kappa_f(t') \cdot \left(v_f(x,y,t') \cdot \rho_f(x,y,t') \right) \, dt' \tag{11}$$

This equation models the temporal growth of wildfire-affected area $\Delta A_{f,t}$ as an integral of the fire propagation rate ($v_f(x,y,t')$) and fuel density $\rho_f(x,y,t')$ over time t, scaled by a growth coefficient $\kappa_f(t')$.

$$\sum_{f \in \mathcal{F}} \left(\Psi_{f,t}^{\text{water}} + \Psi_{f,t}^{\text{equipment}} \right) \leq R_{f,t}^{\max} \tag{12}$$

This constraint limits the total firefighting resources ($\Psi_{f,t}^{\text{water}}$ for water and $\Psi_{f,t}^{\text{equipment}}$ for equipment) used for fire f during time t to a maximum resource availability $R_{f,t}^{\max}$.

$$\mathbb{P}\left(\Phi_{n,t}^{\text{failure}} > \xi_{n,t}^{\text{threshold}} \right) \leq \delta_n \tag{13}$$

This constraint models the probability of grid infrastructure failure ($\Phi_{n,t}^{\text{failure}}$) exceeding a vulnerability threshold ($\xi_{n,t}^{\text{threshold}}$) for node n, ensuring that the risk remains within acceptable limits δ_n.

$$\sum_{n \in \mathcal{C}} \left(\sigma_{n,t}^{\text{crit}} \cdot \Xi_{n,t} \right) \geq \Theta^{\min} \tag{14}$$

This equation prioritizes resource allocation for critical loads ($\Xi_{n,t}$) such as hospitals and shelters, ensuring their operation exceeds a minimum resilience threshold $\Theta^{\min}$.

$$T_{k,t}^{\max} = \frac{T^{\text{ambient}}}{1 + \alpha_k^{\text{heat}} \cdot \Phi_{k,t}^{\text{line}}} \tag{15}$$

This constraint defines the maximum operational temperature ($T_{k,t}^{\max}$) of transmission line k during time t, considering ambient temperature (T^{ambient}) and heat load $\Phi_{k,t}^{\text{line}}$, scaled by heat sensitivity α_k^{heat}.

$$\eta_{b,t} = \eta_b^{\text{base}} - \beta_{b,t}^{\text{wildfire}} \cdot \Phi_{b,t}^{\text{stress}} \tag{16}$$

This equation models the degradation of battery performance ($\eta_{b,t}$) as a function of wildfire-induced stress $\Phi_{b,t}^{\text{stress}}$, with degradation sensitivity $\beta_{b,t}^{\text{wildfire}}$.

$$P_{c,t}^{\text{evac}} = \gamma_{c,t}^{\text{rate}} \cdot N_{c,t}^{\text{evac}} \tag{17}$$

This equation predicts the energy demand for community evacuation ($P_{c,t}^{\text{evac}}$), based on the evacuation rate ($\gamma_{c,t}^{\text{rate}}$) and the number of evacuees ($N_{c,t}^{\text{evac}}$) in community c.

$$\Delta A_{f,t} = \alpha_f^{\text{wind}} \cdot W_{f,t} \cdot \cos(\theta_{f,t}) + \alpha_f^{\text{fuel}} \cdot \Lambda_{f,t} \tag{18}$$

This constraint models wind-driven fire spread, incorporating the influence of wind speed ($W_{f,t}$), direction ($\cos(\theta_{f,t})$), and fuel density ($\Lambda_{f,t}$), with respective scaling factors α_f^{wind} and α_f^{fuel}.

$$\eta_{n,t}^{\text{PV}} = \eta_{n,t}^{\text{base}} \cdot \left(1 - \sigma_{n,t}^{\text{smoke}} \cdot \exp\left(-\tau_{n,t}^{\text{density}} \cdot \left(1 + \kappa_{n,t}^{\text{absorption}} \cdot \Phi_{n,t}^{\text{fire}} \right) \right) \right) \tag{19}$$

This equation models the impact of smoke interference on solar photovoltaic (PV) efficiency, where $\eta_{n,t}^{\text{PV}}$ represents the PV efficiency at node n and time t. The base efficiency, $\eta_{n,t}^{\text{base}}$, is reduced by a factor accounting for smoke density ($\tau_{n,t}^{\text{density}}$), smoke absorption characteristics ($\kappa_{n,t}^{\text{absorption}}$), and fire intensity ($\Phi_{n,t}^{\text{fire}}$), modulated by the exponential decay factor $\exp\left(-\tau_{n,t}^{\text{density}}\right)$. The smoke-related efficiency loss, $\sigma_{n,t}^{\text{smoke}}$, dynamically adjusts based on real-time fire conditions.

$$\sum_{r \in \mathcal{R}} \left(\frac{\Phi_{r,t} \cdot \omega_{r,t}^{\text{fire}}}{1 + \xi_{r,t}^{\text{priority}}} + \frac{\Psi_{r,t}^{\text{water}}}{1 + \zeta_{r,t}^{\text{resource}}} \right) \leq \Theta_t^{\text{resource}} \tag{20}$$

This equation defines the dynamic allocation of water and energy resources during wildfires. The first term prioritizes fire intensity ($\Phi_{r,t}$) relative to fire importance ($\omega_{r,t}^{\text{fire}}$) and priority weights ($\xi_{r,t}^{\text{priority}}$). The second term distributes available water resources ($\Psi_{r,t}^{\text{water}}$) based on resource sensitivity ($\zeta_{r,t}^{\text{resource}}$). The total allocation cannot exceed the system-wide resource availability, $\Theta_t^{\text{resource}}$, ensuring equitable distribution during critical wildfire events.

$$\sum_{k \in \mathcal{K}} \mathcal{F}_{k,t}^{\text{flow}} = 0, \quad \forall t \in T \text{ if } \Phi_t^{\text{wildfire}} \geq \Theta^{\text{island}} \tag{21}$$

This equation enforces microgrid islanding conditions. When wildfire intensity (Φ_t^{wildfire}) exceeds a predefined threshold (Θ^{island}), energy flow ($\mathcal{F}_{k,t}^{\text{flow}}$) from the external grid is reduced to zero, ensuring autonomous operation of the microgrid without external interference.

$$\mathbb{I}\left(\Omega_{n,t}^{\text{distance}} \leq \Lambda^{\text{risk}} \right) \cdot \Phi_{n,t}^{\text{status}} = 0, \quad \forall n \in \mathcal{N},\ t \in T \tag{22}$$

This equation models wildfire risk zones, where the indicator function $\mathbb{I}$ deactivates grid component operation ($\Phi_{n,t}^{\text{status}}$) for any node n within a high-risk zone ($\Omega_{n,t}^{\text{distance}} \leq \Lambda^{\text{risk}}$). This ensures that components near wildfire perimeters are shut down to minimize damage.

$$\Delta x_{f,t}^{\text{topo}} = \beta_f^{\text{elev}} \cdot \nabla h_{f,t} \cdot \cos(\theta_{f,t}) + \gamma_f^{\text{slope}} \cdot \nabla s_{f,t} \cdot \sin(\theta_{f,t}) \tag{23}$$

This equation accounts for topography-based fire spread by combining the elevation gradient ($\nabla h_{f,t}$) and slope gradient ($\nabla s_{f,t}$) with respective coefficients (β_f^{elev} and γ_f^{slope}), modulated by the directionality of fire propagation ($\cos(\theta_{f,t})$ and $\sin(\theta_{f,t})$).

$$q_{e,t} = \sigma_e^{\text{material}} \cdot \left(T_{e,t}^{\text{fire}} - T_{e,t}^{\text{ambient}} \right) + \lambda_{e,t} \cdot \Phi_{e,t}^{\text{heat}} \tag{24}$$

This equation models the heat flux $q_{e,t}$ experienced by grid equipment e, driven by temperature differences between fire conditions ($T_{e,t}^{\text{fire}}$) and ambient conditions ($T_{e,t}^{\text{ambient}}$), scaled by material conductivity $\sigma_e^{\text{material}}$. An additional term incorporates the intensity of fire-induced heat transfer ($\lambda_{e,t} \cdot \Phi_{e,t}^{\text{heat}}$).

$$\mathbb{P}\left(\Phi_{n,t}^{\text{ignite}} \geq \xi_{n,t}^{\text{threshold}} \right) = 1 - \exp\left(-\rho_{n,t} \cdot \Delta d_{n,t}^{\text{fire}} \right) \tag{25}$$

This equation models the ignition probability of infrastructure components ($\Phi_{n,t}^{\text{ignite}}$) based on their proximity to fire sources ($\Delta d_{n,t}^{\text{fire}}$) and material susceptibility ($\rho_{n,t}$). The exponential decay factor ensures realistic probabilities for ignition risks.

$$\mathcal{I}_{f,t}^{\text{intensity}} = \mathcal{I}_{f,t-1}^{\text{intensity}} \cdot \left(1 - \alpha_{f,t}^{\text{firefight}} \cdot \Psi_{f,t}^{\text{water}} \right) \tag{26}$$

This equation reduces wildfire intensity ($\mathcal{I}_{f,t}^{\text{intensity}}$) over time by incorporating firefighting actions. The term $\alpha_{f,t}^{\text{firefight}} \cdot \Psi_{f,t}^{\text{water}}$ captures the effectiveness of water resources applied to suppress the fire.

$$\sum_{t=1}^{T} \Psi_t^{\text{water}} \leq \Psi^{\text{capacity}} \tag{27}$$

This constraint ensures that the total water usage (Ψ_t^{water}) for firefighting over time T does not exceed the available water reservoir capacity (Ψ^{capacity}), maintaining resource sustainability.

$$\sum_{f \in \mathcal{F}} \left(A_{f,t}^{\text{containment}} \cdot \kappa_f^{\text{break}} \cdot \mathcal{E}_{f,t} \right) \geq \Theta_t^{\text{wildfire}} \tag{28}$$

This equation models wildfire containment effectiveness, requiring that the combined impact of containment area ($A_{f,t}^{\text{containment}}$), firebreak efficiency (κ_f^{break}), and suppression efforts ($\mathcal{E}_{f,t}$) exceeds a minimum threshold ($\Theta_t^{\text{wildfire}}$).

$$P_{n,t}^{\text{renewable}} = \mu_{n,t}^{\text{expected}} \pm \Delta P_{n,t}^{\text{stochastic}} \tag{29}$$

This equation incorporates stochastic variations in renewable energy generation ($P_{n,t}^{\text{renewable}}$), centered on expected output ($\mu_{n,t}^{\text{expected}}$) and adjusted by uncertainty factors ($\Delta P_{n,t}^{\text{stochastic}}$) to account for wildfire impacts.

$$\sum_{c\in\mathscr{C}}\left(\Phi_{c,t}^{\text{demand}}\cdot\mathbb{I}(\Omega_{c,t}\le\Lambda^{\text{evac}})\right)\le\Theta_t^{\text{supply}} \tag{30}$$

This equation ensures that the total energy demand ($\Phi_{c,t}^{\text{demand}}$) of evacuation centers ($c\in\mathscr{C}$) within the evacuation zone threshold (Λ^{evac}) is met by the available energy supply (Θ_t^{supply}) during time t.

$$\epsilon_{e,t}^{\text{stress}}=\sigma_e^{\text{material}}\cdot\left(T_{e,t}^{\text{fire}}-T_{e,t}^{\text{ambient}}\right)^2+\lambda_{e,t}\cdot\Phi_{e,t}^{\text{load}} \tag{31}$$

This equation models thermal stress ($\epsilon_{e,t}^{\text{stress}}$) on grid components ($e$) due to temperature-induced material degradation. It includes quadratic temperature effects from fire conditions ($T_{e,t}^{\text{fire}}$) and load-induced stress ($\Phi_{e,t}^{\text{load}}$) scaled by thermal sensitivity coefficients.

$$\sum_{t=1}^{T}\left(\eta_{g,t}^{\text{emission}}\cdot\xi_{g,t}^{\text{fuel}}\cdot P_{g,t}^{\text{diesel}}\right)\le\Theta^{\text{emission}} \tag{32}$$

This equation enforces emission constraints from diesel generators. The total carbon emissions ($\eta_{g,t}^{\text{emission}}\cdot\xi_{g,t}^{\text{fuel}}\cdot P_{g,t}^{\text{diesel}}$) across all generators g and time T must remain below a predefined limit (Θ^{emission}).

$$\Phi_t^{\text{threat}}=\sum_{f\in\mathscr{F}}\left(\alpha_{f,t}^{\text{intensity}}\cdot\kappa_{f,t}^{\text{spread}}\cdot A_{f,t}^{\text{fire}}\right) \tag{33}$$

This equation dynamically updates wildfire threat levels (Φ_t^{threat}) based on fire intensity ($\alpha_{f,t}^{\text{intensity}}$), spread rate ($\kappa_{f,t}^{\text{spread}}$), and affected area ($A_{f,t}^{\text{fire}}$) for all fires ($f\in\mathscr{F}$).

$$\sum_{f\in\mathscr{F}}\left(\Psi_{f,t}^{\text{retardant}}\cdot\mathbb{I}(\Phi_{f,t}^{\text{area}}\le\Lambda^{\text{retardant}})\right)\le\Psi^{\text{capacity}} \tag{34}$$

This equation models the application of fire retardants, ensuring that the total retardant usage ($\Psi_{f,t}^{\text{retardant}}$) for fires within a manageable area threshold ($\Phi_{f,t}^{\text{area}}\le\Lambda^{\text{retardant}}$) remains within the maximum capacity (Ψ^{capacity}).

$$\sum_{m\in\mathscr{M}}\left(W_{m,t}^{\text{essential}}+W_{m,t}^{\text{loss}}\right)\le W_t^{\text{avail}} \tag{35}$$

This equation ensures community water consumption by limiting the sum of essential usage ($W_{m,t}^{\text{essential}}$) and losses ($W_{m,t}^{\text{loss}}$) for all resources m to the available water supply (W_t^{avail}).

$$\sum_{k\in\mathscr{K}}\mathscr{F}_{k,t}^{\text{flow}}+\mathbb{I}(\Phi_{k,t}^{\text{fire}}>\Lambda^{\text{risk}})\cdot\Phi_{k,t}^{\text{reconfig}}=0 \tag{36}$$

This equation models grid reconfiguration under fire threats. It ensures that the flow along transmission lines ($\mathscr{F}_{k,t}^{\text{flow}}$) and reconfiguration efforts ($\Phi_{k,t}^{\text{reconfig}}$) adapt dynamically based on fire risk levels ($\Phi_{k,t}^{\text{fire}}$) exceeding a critical threshold (Λ^{risk}).

$$P_{c,t}^{\text{demand}}=\mu_{c,t}^{\text{expected}}\pm\Delta P_{c,t}^{\text{stochastic}} \tag{37}$$

This equation predicts energy demand for fire-induced evacuations ($P_{c,t}^{\text{demand}}$), accounting for expected demand ($\mu_{c,t}^{\text{expected}}$) and uncertainty ($\Delta P_{c,t}^{\text{stochastic}}$) due to varying evacuation scenarios.

$$\sum_{n\in\mathscr{N}}\Phi_{n,t}^{\text{share}}=\sum_{m\in\mathscr{M}}\Phi_{m,t}^{\text{receive}},\quad\forall t\in T \tag{38}$$

This equation ensures inter-microgrid energy sharing during emergencies. The total energy shared ($\Phi_{n,t}^{\text{share}}$) by one microgrid equals the energy received ($\Phi_{m,t}^{\text{receive}}$) by another, ensuring balanced energy redistribution.

$$v_{f,t}^{\text{wind}}=v_{f,t}^{\text{base}}\cdot\left(1+\alpha_{f,t}^{\text{wind}}\cdot W_{f,t}^{\text{speed}}\cdot\cos(\theta_{f,t})\right) \tag{39}$$

This equation models wind-driven fire acceleration. The fire propagation speed ($v_{f,t}^{\text{wind}}$) is amplified by the base fire speed ($v_{f,t}^{\text{base}}$) and scaled by the wind speed ($W_{f,t}^{\text{speed}}$) and direction ($\cos(\theta_{f,t})$) through a wind sensitivity factor ($\alpha_{f,t}^{\text{wind}}$).

$$\sum_{r\in\mathscr{R}}\left(\Phi_{r,t}^{\text{repair}}+\Psi_{r,t}^{\text{resource}}\cdot\kappa_{r,t}^{\text{priority}}\right)\le\Theta_t^{\text{recovery}} \tag{40}$$

This equation defines the post-fire recovery model, ensuring that the total allocation of repair resources ($\Phi_{r,t}^{\text{repair}}$) and prioritized restoration efforts ($\Psi_{r,t}^{\text{resource}}\cdot\kappa_{r,t}^{\text{priority}}$) remains within the recovery capacity ($\Theta_t^{\text{recovery}}$).

4. Method

The methodology section builds upon the mathematical framework by detailing the computational strategies, data integration processes, and validation techniques employed in this research. Wildfires are highly dynamic phenomena, requiring methodologies that are not only computationally efficient but also capable of adapting to real-time changes in environmental and operational conditions. This section provides a step-by-step outline of the approaches used to simulate, optimize, and evaluate the proposed system. Central to the methodology is the use of digital twin technology, which serves as a real-time virtual representation of the physical system. The digital twin framework enables continuous monitoring and simulation of wildfire behavior, energy system performance, and resource allocation dynamics. This approach is increasingly recognized in disaster management contexts for its ability to synthesize multisource data and provide predictive analytics (Li et al., 2025d). Advanced algorithms, including real-time optimization for resource deployment and machine learning models for fire spread prediction, are integrated into this framework to enhance decision-making under uncertainty. Techniques such as reinforcement learning and metaheuristics have shown promise in capturing the stochastic and spatially distributed nature of wildfire impacts (Li et al., 2025c). Furthermore, this section elaborates on the incorporation of real-world data, including topographical maps, weather patterns, and historical fire events, into the model. Computational strategies such as parallel processing and scenario-based DRO optimization are employed to ensure scalability and efficiency. Validation of the methodology is carried out through case studies based on recent wildfire events in Los Angeles, demonstrating the framework's ability to optimize resource allocation, improve system resilience, and support post-fire recovery. Results are benchmarked against baseline strategies, highlighting substantial improvements in energy reliability and water resource coordination. This comprehensive methodology ensures that the proposed framework is both practical and scalable for real-world applications, complementing current trends in wildfire-aware infrastructure design (Wang et al., 2025).

Fig. 1 illustrates a two-layer digital-twin-assisted architecture designed to coordinate wildfire, energy, and water systems under dynamic environmental conditions. The upper layer is responsible for predictive analytics and strategic decision-making. It integrates real-time environmental data, wildfire propagation modeling, and forecasts of energy load and water demand. These inputs feed into a digital twin that simulates the coupled dynamics of wildfire spread, infrastructure status, and resource availability. Leveraging these simulations, a distributionally robust optimizer based on the Wasserstein ambiguity set generates actionable setpoints. These setpoints include optimal energy allocation, water routing, fire containment strategies, and resource prioritization policies. A temporal consistency check ensures the optimizer's output remains aligned with evolving conditions. The lower layer focuses on operational response. It executes setpoints through three coordinated modules. The wildfire management block utilizes feedback such as frequency deviation (ω), rate of change of frequency (RoCoF), and voltage-flow parameters to trigger protective actions. The resource coordination block orchestrates battery dispatch, virtual inertia control (if applicable), and emergency pump deployment to balance supply

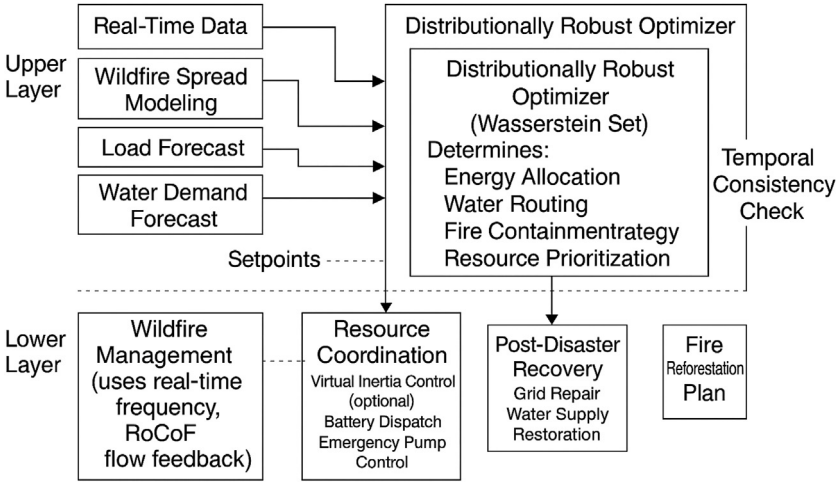


Fig. 1. Two-layer digital-twin-assisted wildfire-energy-water management architecture.

and demand. Finally, the post-disaster recovery module ensures the restoration of critical infrastructure, such as power and water networks, and initiates long-term ecological recovery including reforestation planning. Together, the two layers form a closed-loop cyber–physical framework capable of enhancing system resilience before, during, and after wildfire disasters.

$$\mathscr{D}_t^{\text{twin}} = \sum_{n\in\mathscr{N}} \left(\boldsymbol{\Phi}_{n,t}^{\text{water}} \cdot \boldsymbol{\Psi}_{n,t}^{\text{energy}} \cdot \eta_{n,t}^{\text{eff}}\right) - \sum_{k\in\mathscr{K}} \mathscr{F}_{k,t}^{\text{loss}} + \sum_{m\in\mathscr{M}} \left(\rho_{m,t}^{\text{fire}} \cdot \boldsymbol{\Phi}_{m,t}^{\text{demand}}\right), \tag{41}$$

This equation integrates water–energy nexus modeling into the digital twin framework, balancing water ($\boldsymbol{\Phi}_{n,t}^{\text{water}}$) and energy ($\boldsymbol{\Psi}_{n,t}^{\text{energy}}$) usage with efficiency losses ($\eta_{n,t}^{\text{eff}}$) and fire-induced demand impacts ($\rho_{m,t}^{\text{fire}}$).

$$v_{f,t} = \mathscr{F}\left(W_{f,t}, \rho_{f,t}, \Lambda_{f,t}\right) \tag{42}$$

This equation predicts fire spread using real-time inputs, including wind conditions ($W_{f,t}$), vegetation density ($\rho_{f,t}$), and fire fuel availability ($\Lambda_{f,t}$) through a functional mapping $\mathscr{F}$.

$$\boldsymbol{\Phi}_{k,t}^{\text{topology}} = \mathbb{I}(\boldsymbol{\Phi}_{k,t}^{\text{fire}} > \Lambda^{\text{risk}}) \cdot \boldsymbol{\Phi}_{k,t}^{\text{reconfig}} \tag{43}$$

This equation models fire-induced grid topology changes, where the indicator function $\mathbb{I}$ reconfigures grid line status ($\boldsymbol{\Phi}_{k,t}^{\text{topology}}$) if the fire intensity ($\boldsymbol{\Phi}_{k,t}^{\text{fire}}$) exceeds a critical risk threshold (Λ^{risk}).

$$\vec{W}_{f,t} = W_{f,t}^{\text{speed}} \cdot \left(\cos(\theta_{f,t})\hat{i} + \sin(\theta_{f,t})\hat{j}\right) \tag{44}$$

This equation simulates wind vectors, decomposing wildfire-driven wind conditions into directional components ($\cos(\theta_{f,t})$ and $\sin(\theta_{f,t})$) for accurate fire spread modeling.

$$\min_{\boldsymbol{\Phi}} \ \mathbb{E}_{\xi\sim\mathscr{P}}\left[\mathscr{C}(\boldsymbol{\Phi},\xi)\right] + \kappa \cdot \sup_{\mathscr{Q}\in\mathscr{U}} \mathbb{E}_{\xi\sim\mathscr{Q}}\left[\mathscr{C}(\boldsymbol{\Phi},\xi)\right] \tag{45}$$

This equation defines the DRO formulation for resource allocation, optimizing under distributional uncertainty. The objective combines expected cost ($\mathbb{E}_{\xi\sim\mathscr{P}}$) and worst-case cost ($\sup_{\mathscr{Q}\in\mathscr{U}}$) to ensure robust solutions.

$$\epsilon_{e,t} = \sigma_e^{\text{thermal}} \cdot \left(T_{e,t}^{\text{fire}} - T_{e,t}^{\text{ambient}}\right)^2 \tag{46}$$

This equation models thermal stress on grid components, with material sensitivity $\sigma_e^{\text{thermal}}$ and temperature differentials between fire ($T_{e,t}^{\text{fire}}$) and ambient conditions ($T_{e,t}^{\text{ambient}}$).

$$\boldsymbol{\Psi}_t^{\text{water}} = \sum_{f\in\mathscr{F}} \left(\kappa_{f,t}^{\text{firefight}} \cdot \mathscr{J}_{f,t}\right) \tag{47}$$

This equation forecasts water consumption for firefighting, summing firefighting efforts ($\mathscr{J}_{f,t}$) scaled by fire-specific water use coefficients ($\kappa_{f,t}^{\text{firefight}}$).

$$\boldsymbol{\Phi}_t^{\text{risk}} = \mathscr{F}\left(\boldsymbol{\Phi}_t^{\text{fire}}, \Lambda^{\text{boundary}}, W_{f,t}\right) \tag{48}$$

This equation dynamically updates wildfire risk zones by integrating fire intensity, containment boundaries ($\Lambda^{\text{boundary}}$), and wind conditions.

$$P_{n,t}^{\text{renewable}} = \mu_{n,t}^{\text{expected}} + \Delta P_{n,t}^{\text{stochastic}} \tag{49}$$

This equation models stochastic renewable generation by combining expected generation with uncertainty adjustments ($\Delta P_{n,t}^{\text{stochastic}}$).

$$\mathscr{D}_t^{\text{spatial}} = \sum_{f\in\mathscr{F}} \left(A_{f,t}^{\text{fire}} \cdot \kappa_{f,t}^{\text{spread}}\right) \tag{50}$$

This equation integrates spatial fire data into the digital twin, summing fire areas ($A_{f,t}^{\text{fire}}$) weighted by spread coefficients ($\kappa_{f,t}^{\text{spread}}$).

$$\frac{\partial \boldsymbol{\Phi}_{n,t}^{\text{resilience}}}{\partial \mathscr{J}_{f,t}} = \eta_{n,t}^{\text{sensitivity}} \tag{51}$$

This equation models sensitivity analysis of resilience metrics ($\boldsymbol{\Phi}_{n,t}^{\text{resilience}}$) relative to fire intensity ($\mathscr{J}_{f,t}$).

$$\mathscr{L}_t^{\text{water-energy}} = \boldsymbol{\Phi}_t^{\text{water}} \cdot \boldsymbol{\Psi}_t^{\text{energy}} \tag{52}$$

This equation models interdependencies in the water–energy nexus, linking water usage ($\boldsymbol{\Phi}_t^{\text{water}}$) and energy consumption ($\boldsymbol{\Psi}_t^{\text{energy}}$).

$$P_{c,t}^{\text{evac}} = \mu_{c,t}^{\text{expected}} + \Delta P_{c,t}^{\text{uncertainty}} \tag{53}$$

This equation predicts evacuation-triggered energy demand, incorporating both expected demand ($\mu_{c,t}^{\text{expected}}$) and uncertainty ($\Delta P_{c,t}^{\text{uncertainty}}$).

$$\min_{\boldsymbol{\Phi}_{f,t},\boldsymbol{\Psi}_{f,t}} \sum_{f\in\mathscr{F}} \left[\alpha_{f,t}^{\text{firefight}} \cdot \boldsymbol{\Psi}_{f,t}^{\text{water}} + \beta_{f,t}^{\text{equipment}} \cdot \boldsymbol{\Psi}_{f,t}^{\text{resources}}\right] + \sum_{f\in\mathscr{F}} \left[\lambda_{f,t}^{\text{response}} \cdot \left(\mathscr{J}_{f,t}^{\text{intensity}} - \gamma_{f,t}^{\text{threshold}}\right)^2 + \eta_{f,t}^{\text{allocation}} \cdot \Delta \boldsymbol{\Phi}_{f,t}^{\text{spread}}\right], \tag{54}$$

This equation models real-time optimization for firefighting resource allocation by minimizing the combined costs of water usage ($\boldsymbol{\Psi}_{f,t}^{\text{water}}$), equipment deployment ($\boldsymbol{\Psi}_{f,t}^{\text{resources}}$), and response delays. The terms include penalties for fire intensity exceeding critical thresholds

$(\mathcal{I}_{f,t}^{\text{intensity}} - \gamma_{f,t}^{\text{threshold}})$ and inefficiencies in resource distribution $(\eta_{f,t}^{\text{allocation}} \cdot \Delta\Phi_{f,t}^{\text{spread}})$.

$$\eta_{b,t}^{\text{performance}} = \eta_{b,t}^{\text{base}} - \alpha_{b,t}^{\text{thermal}} \cdot \left(T_{b,t}^{\text{fire}} - T_{b,t}^{\text{ambient}}\right)^2 - \beta_{b,t}^{\text{stress}} \cdot \Phi_{b,t}^{\text{load}} \tag{55}$$

This equation models battery performance under wildfire-induced stress, where $\eta_{b,t}^{\text{performance}}$ depends on the base performance $(\eta_{b,t}^{\text{base}})$, thermal effects $(\alpha_{b,t}^{\text{thermal}})$, and load-induced stress $(\beta_{b,t}^{\text{stress}} \cdot \Phi_{b,t}^{\text{load}})$ during fire conditions.

$$\sigma_{n,t}^{\text{smoke}} = \tau_{n,t}^{\text{density}} \cdot \exp\left(-\kappa_{n,t}^{\text{dispersal}} \cdot \Phi_{n,t}^{\text{wind}}\right) + \gamma_{n,t}^{\text{particulate}} \cdot \Phi_{n,t}^{\text{fire}} \tag{56}$$

This equation models smoke density for photovoltaic efficiency reduction, incorporating particle density $(\tau_{n,t}^{\text{density}})$, dispersal effects due to wind speed $(\kappa_{n,t}^{\text{dispersal}} \cdot \Phi_{n,t}^{\text{wind}})$, and additional fire-driven particulate generation $(\gamma_{n,t}^{\text{particulate}} \cdot \Phi_{n,t}^{\text{fire}})$.

$$\mathcal{R}_t^{\text{dynamic}} = \sum_{r \in \mathcal{R}} \Phi_{r,t}^{\text{demand}} \cdot \frac{\kappa_{r,t}^{\text{priority}}}{1 + \lambda_{r,t}^{\text{delay}}} + \sum_{n \in \mathcal{N}} \Psi_{n,t}^{\text{reallocate}} \cdot \eta_{n,t}^{\text{efficiency}} \tag{57}$$

This equation defines a dynamic resource reallocation algorithm by balancing demand priority $(\Phi_{r,t}^{\text{demand}} \cdot \kappa_{r,t}^{\text{priority}})$ and reallocation efficiency $(\Psi_{n,t}^{\text{reallocate}} \cdot \eta_{n,t}^{\text{efficiency}})$, penalizing delays $(\lambda_{r,t}^{\text{delay}})$.

$$q_{e,t}^{\text{thermal}} = \sigma_e^{\text{resistance}} \cdot \left(T_{e,t}^{\text{fire}} - T_{e,t}^{\text{ambient}}\right)^2 + \lambda_{e,t} \cdot \Phi_{e,t}^{\text{heatload}} \tag{58}$$

This equation models thermal resistance for grid infrastructure, with resistance loss scaling quadratically with temperature $(T_{e,t}^{\text{fire}} - T_{e,t}^{\text{ambient}})$ and accounting for heat load effects $(\Phi_{e,t}^{\text{heatload}})$.

$$\min_{\Phi} \mathbb{E}_{\xi \sim \mathcal{P}} \left[\mathcal{C}(\Phi, \xi) + \kappa \cdot \sum_{f \in \mathcal{F}} \left(\Psi_{f,t}^{\text{suppression}} \cdot \mathcal{I}_{f,t}^{\text{intensity}} \right) \right] \tag{59}$$

This DRO-based equation integrates fire suppression strategies into resource optimization by minimizing expected costs $(\mathcal{C}(\Phi, \xi))$ and fire suppression effects $(\Psi_{f,t}^{\text{suppression}} \cdot \mathcal{I}_{f,t}^{\text{intensity}})$.

$$\Phi_{c,t}^{\text{evacuation}} = \frac{\Phi_{c,t}^{\text{population}} \cdot \eta_{c,t}^{\text{criticality}}}{1 + \lambda_{c,t}^{\text{distance}}} \tag{60}$$

This algorithm prioritizes evacuation zones by allocating resources based on population size $(\Phi_{c,t}^{\text{population}})$, criticality factors $(\eta_{c,t}^{\text{criticality}})$, and distance penalties $(\lambda_{c,t}^{\text{distance}})$.

$$\mathcal{C}_t^{\text{shared}} = \sum_{m \in \mathcal{M}} \Phi_{m,t}^{\text{send}} \cdot \eta_{m,t}^{\text{efficiency}} - \sum_{n \in \mathcal{N}} \Phi_{n,t}^{\text{receive}} \cdot \lambda_{n,t}^{\text{loss}} \tag{61}$$

This equation models multi-microgrid energy sharing, balancing sent $(\Phi_{m,t}^{\text{send}})$ and received $(\Phi_{n,t}^{\text{receive}})$ energy while accounting for efficiency $(\eta_{m,t}^{\text{efficiency}})$ and losses $(\lambda_{n,t}^{\text{loss}})$.

$$\mathcal{S}_t^{\text{DRO}} = \sup_{\mathcal{Q} \in \mathcal{U}} \mathbb{E}_{\xi \sim \mathcal{Q}} \left[\mathcal{C}(\Phi, \xi)\right] + \inf_{\mathcal{P} \in \mathcal{U}} \mathbb{E}_{\xi \sim \mathcal{P}} \left[\mathcal{C}(\Phi, \xi)\right] \tag{62}$$

This DRO scenario generation equation ensures robust optimization for wildfire uncertainties, balancing worst-case (sup) and best-case (inf) expectations across uncertain distributions.

$$\Phi_t^{\text{postfire}} = \sum_{r \in \mathcal{R}} \Phi_{r,t}^{\text{repair}} \cdot \eta_{r,t}^{\text{efficiency}} + \Psi_{r,t}^{\text{resource}} \cdot \kappa_{r,t}^{\text{priority}} \tag{63}$$

This equation optimizes post-fire recovery by prioritizing repairs $(\Phi_{r,t}^{\text{repair}})$, resource allocation $(\Psi_{r,t}^{\text{resource}})$, and efficiency enhancements $(\eta_{r,t}^{\text{efficiency}})$ based on priority weights $(\kappa_{r,t}^{\text{priority}})$.

5. Results

The case study focuses on the ongoing Palisades Fire in Los Angeles, utilizing both real-time and historical data sources to validate the effectiveness and realism of the proposed framework. As of January 20, 2025, the wildfire has burned more than 24,000 acres, destroyed over 12,300 structures, and led to the evacuation of nearly 200,000 residents. Spatial data are primarily derived from United States Geological Survey (USGS) fire perimeters and high-resolution satellite imagery provided by NASA's MODIS and VIIRS instruments (Zhou et al., 2025). Wind speeds exceeding 100 mph in mountainous areas are captured from NOAA's National Weather Service, while smoke density and local weather conditions are recorded by the South Coast Air Quality Management District (SCAQMD). The FARSITE simulator is used to model wildfire dynamics, with calibration informed by vegetation cover and topography data from CAL FIRE. Within the affected regions, energy infrastructure includes distributed microgrids comprising 150 nodes. These networks integrate solar PV, battery storage, and diesel backup units, with an aggregated PV capacity of 100 MW and battery systems totaling 200 MWh of storage. Due to wildfire smoke interference, real-time measurements report a decline of up to 60% in PV efficiency, a phenomenon previously observed in similar fire events (Kadir et al., 2021). Battery discharges peaked at 75 MW during emergency periods, and diesel generators — covering 20% of peak demand — introduce 1.2 kg/kWh of emissions, necessitating integrated emissions modeling to assess environmental tradeoffs. Water resources are also explicitly incorporated, with reservoirs storing up to 80 million gallons and firefighting demands exceeding 15 million gallons per day. Simulation execution spans several integrated platforms: Pyomo and Gurobi Optimizer 9.5 for mixed-integer programming, MATLAB Simulink and Unity 3D for digital twin rendering, and FARSITE (augmented by WindNinja) for terrain-informed fire modeling. The simulation environment runs on a high-performance computing cluster with 256 cores, 2 TB RAM, and NVIDIA A100 GPUs, supporting the generation of 500 stochastic DRO scenarios based on historical fire propagation and renewable variability (Heluany and Gkioulos, 2024). This integrated architecture ensures the case study reflects the operational and environmental complexities involved in wildfire management.

To ensure clarity and reproducibility, this study defines the key initial and operating conditions that govern the integrated simulation environment. Wildfire dynamics are initialized under representative meteorological conditions for Los Angeles in early January, with wind velocity ranging from 40 to 60 mph and ambient temperature set to 34 °C. These values reflect the peak conditions observed during the Palisades Fire scenario. Fire ignition originates from a designated node within the urban-wildland interface, and the fire spread evolves dynamically based on topography and wind influence. The energy system begins with a battery state-of-charge (SoC) initialized at 90%, assuming moderate preparedness levels. Photovoltaic generation at each node is modeled with a baseline efficiency $\eta_{n,t}^{PV} = 18\%$, and a reference operating temperature $T_{\text{ref}} = 25$ °C. Efficiency losses due to smoke interference are captured by a derating coefficient $\sigma_{n,t}^{\text{smoke}}$, which varies temporally with fire progression. Power loads follow representative urban demand profiles, and each node has the flexibility to draw from storage or renewable sources. Water availability is modeled with initial reservoir levels set at 80% of capacity. Sector-specific firefighting demand $W_{m,t}^{\text{essential}}$ is estimated based on projected fire severity and population density. All simulations are executed over a fixed 24-h horizon with a resolution of 5 min per step, enabling high-fidelity temporal tracking of system interdependencies. The complete set of initial conditions is summarized in Table 2 (see Fig. 2).

Fig. 3 illustrates the relationship between smoke density, measured as PM2.5 levels in micrograms per cubic meter, and the efficiency of solar photovoltaic (PV) systems across three different microgrid locations: Location A, Location B, and Location C. The smoke density values range from 50 to 300, with PV efficiency decreasing non-linearly as smoke density increases. For instance, at lower smoke densities around 50, PV systems maintain an average efficiency of approximately 95%. However, as smoke density rises to 200, efficiency decreases to about 72%, and further reductions occur at 300, where efficiency drops to nearly 60%. This trend demonstrates the significant impact

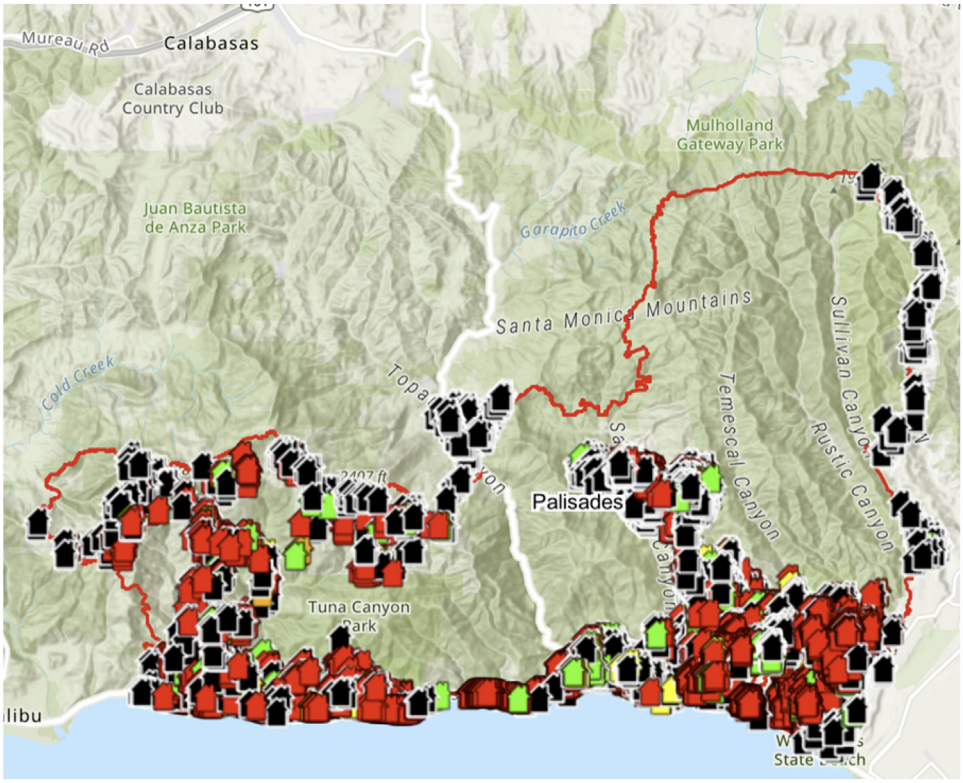


Fig. 2. Palisades fire structure impact map: Damage assessment and perimeter visualization.

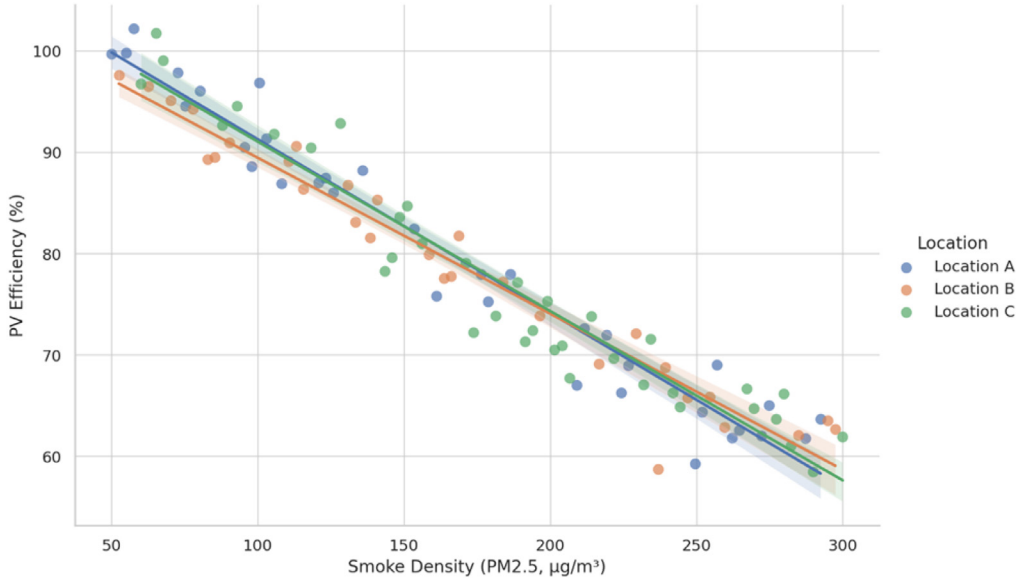


Fig. 3. Impact of smoke density on solar PV efficiency across locations.

of wildfire-induced smoke on renewable energy performance, especially during periods of high particulate concentration. The figure also highlights variability among the three microgrid locations. Location A, characterized by relatively stable environmental conditions, exhibits a more gradual decline in PV efficiency. Conversely, Location B, affected by higher particulate levels and more volatile weather patterns, shows a sharper decrease in efficiency, particularly between 150 and 250, where efficiency drops by nearly 20 percentage points. Location C demonstrates intermediate behavior, with a noticeable fluctuation in efficiency attributed to variable terrain and smoke dispersal effects. The non-linear regression lines for each location capture these distinctions, showing not only the general downward trend but also site-specific differences due to local conditions such as topography, vegetation density, and wind patterns. This visualization provides critical insights for managing renewable energy systems during wildfire events. The non-linear nature of the trend suggests that incremental increases in smoke density have progressively severe impacts on PV efficiency, particularly beyond the threshold of 200. This finding underscores the importance of integrating real-time air quality monitoring into energy management systems to optimize resource allocation. Additionally, the clear differences between locations indicate that localized strategies are essential for mitigating the effects of wildfire smoke on PV systems.

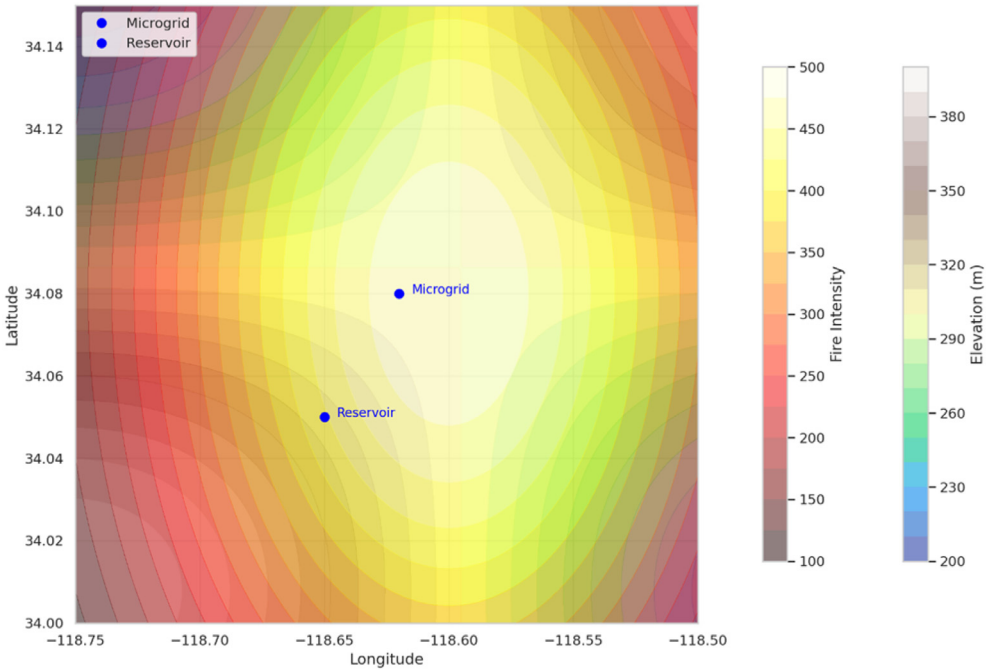


Fig. 4. Topographic fire spread simulation in pacific palisades.

Table 2
Initial simulation parameters.

Symbol	Description	Value
v_{wind}	Initial wind velocity	40–60 mph
$T_{e,t}$	Ambient air temperature	34 °C
SoC_0	Initial battery state of charge	90%
$\eta_{n,t}^{\text{PV}}$	Baseline PV efficiency	18%
T_{ref}	Reference PV temperature	25 °C
$\sigma_{n,t}^{\text{smoke}}$	Smoke derating coefficient	Variable, 0–50%
$W_{m,t}^{\text{avail}}$	Water reservoir initial level	80% capacity
$W_{m,t}^{\text{essential}}$	Essential firefighting water demand	Scenario-based
Δt	Simulation time step	5 min
T_{sim}	Total simulation duration	24 h

By accounting for the unique environmental characteristics of each microgrid, operators can prioritize maintenance, enhance energy storage utilization, and adaptively manage grid resources during wildfire crises.

Fig. 4 provides a detailed simulation of fire spread overlaid on the topographic contours of Pacific Palisades. The topography, represented through contour lines, shows elevation levels ranging from 200 m to 400 m, reflecting the diverse terrain of the region. Fire intensity is visualized as a heatmap with values up to 500 BTU/m^2, indicating the most affected areas. Critical infrastructure points, such as a microgrid located at (−118.62, 34.08) and a reservoir at (−118.65, 34.05), are marked to emphasize their proximity to high-risk zones. The data highlights how the combination of elevation and fire intensity can inform resource allocation for firefighting and infrastructure protection. The simulation reveals a concentrated fire intensity peak near 34.08° latitude and −118.6° longitude, with intensity values declining as the distance from this epicenter increases. The proximity of the microgrid, approximately 200 m from the fire's epicenter, suggests a high risk to energy infrastructure. Similarly, the reservoir located 300 m from the edge of the high-intensity zone faces potential challenges in maintaining water availability for firefighting efforts. This proximity analysis underscores the importance of prioritizing resources for the most critical zones based on geographic and topographic risk factors. By incorporating both topography and fire intensity, this figure demonstrates the spatial dynamics of wildfire spread in the Pacific Palisades area. The inclusion of elevation highlights how slopes and elevation gradients influence fire behavior, such as faster uphill fire spread due to heat rising. The visualization serves as a crucial tool for emergency planning, enabling stakeholders to identify vulnerable areas and strategically deploy resources. The simulation can also be extended to analyze evacuation routes and evaluate the effectiveness of existing firebreaks and barriers. This integrated approach ensures a comprehensive understanding of wildfire impacts and mitigation strategies.

Fig. 5 illustrates the fire spread progression in Pacific Palisades over 24 h, with snapshots captured at four distinct intervals: 6, 12, 18, and 24 h. The underlying topographic data, represented through contour lines, shows elevation variations ranging from 200 m to 400 m, highlighting the hilly terrain of the Santa Monica Mountains. The fire spread is represented as a heatmap overlaid on the topography, with intensity values peaking at 500 BTU/m^2 near the fire origin. Critical infrastructure points, such as a microgrid at (−118.62, 34.08) and a reservoir at (−118.65, 34.05), are marked to emphasize their spatial relationship to the fire spread. The progression reveals distinct fire movement patterns influenced by terrain. At the 6-h mark, the fire is concentrated near its origin, with the intensity diminishing beyond a 500-m radius. By the 12-h mark, the fire spreads upslope, driven by the elevation gradient and prevailing wind patterns, increasing the affected area by approximately 30%. The 18-h snapshot shows a further expansion towards the north, with intensity zones encroaching within 200 m of the microgrid, signaling critical risk. At the 24-h mark, the fire spread reaches its maximum extent in this simulation, with a perimeter extending over 1.5 km and intensity tapering off near the outer boundaries.

Fig. 6 illustrates the dynamic interaction between wind patterns, topography, and fire intensity in Pacific Palisades. The elevation contour lines reveal the region's varied terrain, with elevations ranging from 200 m to 400 m, typical of the Santa Monica Mountains. Fire intensity, represented as a heatmap, peaks at approximately 500 BTU/m^2 near the origin point at latitude 34.08° and longitude −118.6°. The addition of wind vectors, showing speeds of up to 20 m/s, highlights the directional influence of wind on fire spread, particularly in regions with steep elevation gradients. The wind vectors indicate a strong northward and westward component, consistent with Santa Ana wind conditions commonly observed in the Los Angeles area during wildfire events.

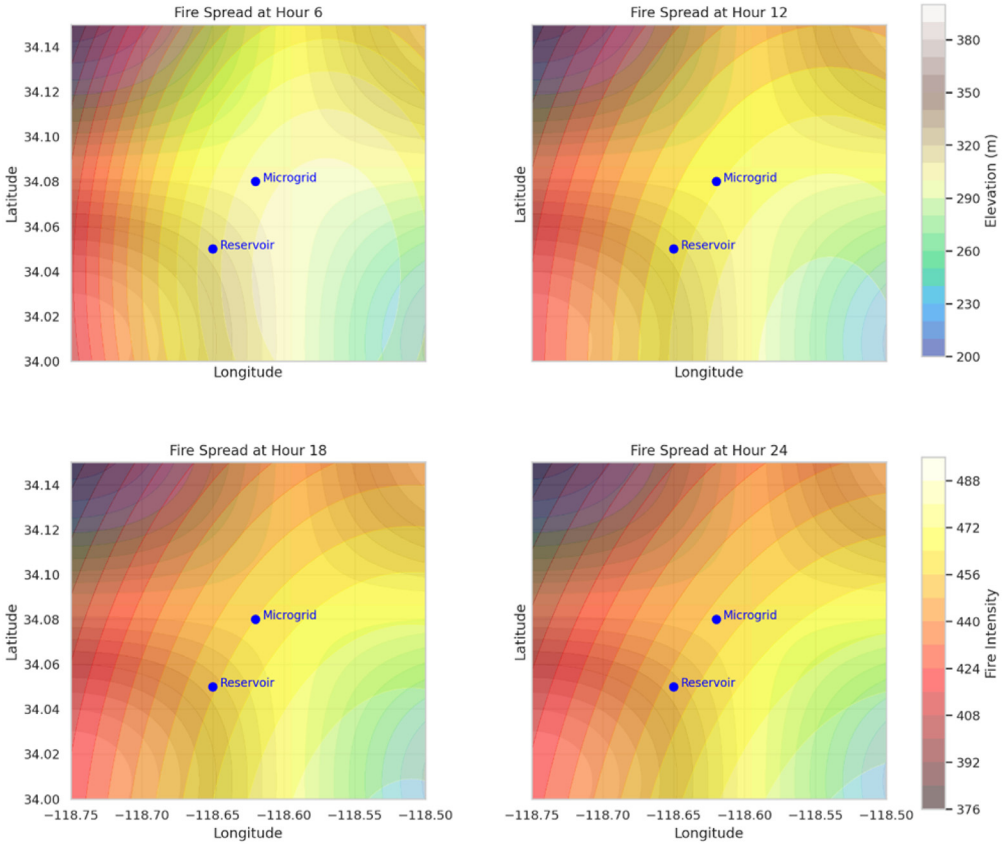


Fig. 5. Temporal fire spread progression in pacific palisades over topographic terrain.

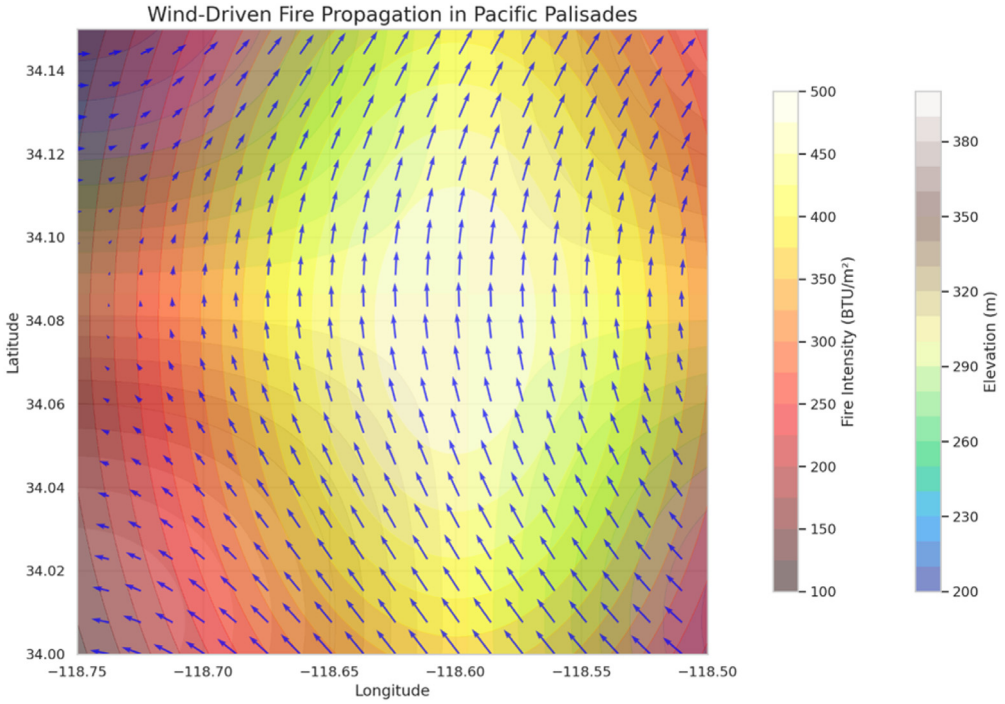


Fig. 6. Wind-driven fire propagation in pacific palisades.

Table 3
Comparison of conventional methods and the proposed framework.

Feature	Conventional methods	Proposed framework
Wildfire modeling	Static fire perimeter or simplified risk zones	Dynamic simulation based on terrain, wind, and vegetation data
Energy system focus	Separate dispatch optimization or contingency analysis	Joint optimization with fire-aware constraints and real-time adaptation
Water resource modeling	Often excluded or treated as fixed input	Explicitly integrated with firefighting and community demand trade-offs
Uncertainty handling	Deterministic or scenario-based without robustness	Distributionally robust optimization with stochastic fire and energy variables
Control parameter tuning	Manually assigned or fixed by rules	Sensitivity-informed selection with real-time feedback compatibility
Decision-making timescale	Strategic or day-ahead planning	Real-time or near-real-time emergency coordination
Critical load prioritization	Not explicitly modeled	Embedded in objective with weight-adjustable structure

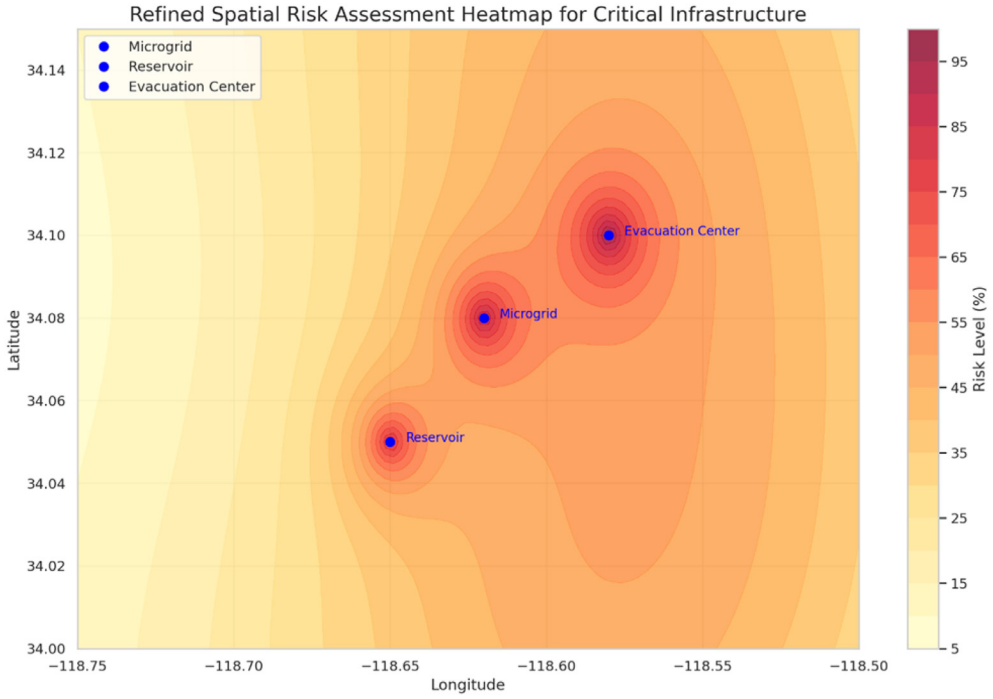


Fig. 7. Spatial risk assessment heatmap for critical infrastructure. (For interpretation of the references to color in this figure legend, the reader is referred to the web version of this article.)

These high-speed winds accelerate fire spread by transporting embers across significant distances, igniting new areas ahead of the primary fire front. For instance, the wind-driven propagation shifts the high-intensity zones by over 500 m within the mapped area. The influence of wind is most pronounced in the northwestern section of the map, where fire intensity overlaps with regions of elevated terrain, amplifying the spread rate.

Fig. 7 presents a refined spatial risk assessment heatmap for critical infrastructure in the wildfire-affected region of Pacific Palisades. The color gradient ranges from light yellow (low risk) to deep red (high risk), representing varying risk levels. The highest-risk zones are concentrated near the fire origin at latitude 34.08° and longitude −118.62°, with risk levels reaching 100%. Surrounding regions experience a gradual decrease in risk, influenced by both proximity to the fire and simulated terrain effects. Critical infrastructure points such as the microgrid, reservoir, and evacuation center are marked to emphasize their exposure to these risks. The localized increase in risk around critical infrastructure points is evident, particularly near the microgrid and reservoir. The microgrid, situated approximately 100 m from the fire origin, faces significant exposure, with a surrounding risk level exceeding 85%. Similarly, the reservoir, located around 300 m from the high-intensity zone, experiences a moderate risk level of 60%–70%. The evacuation center, positioned farther from the fire epicenter, benefits from its relative distance, with surrounding risk levels peaking at 40%. These variations highlight the spatial disparities in risk and the importance of prioritizing protection measures for critical facilities in high-risk zones.

Fig. 8 visualizes the interaction between wildfire intensity, terrain elevation, and infrastructure resilience levels in the Pacific Palisades region. The fire intensity heatmap, represented in shades of red, highlights the epicenter near latitude 34.08° and longitude −118.62°, where intensity peaks at 100%. The surrounding zones show a gradual decline in intensity as distance from the fire origin increases. Overlaid black contour lines indicate terrain elevation, ranging from 200 m to 400 m. The elevation data provides insight into how topography influences fire dynamics, particularly the uphill spread toward the northwestern zones. The resilience levels of critical infrastructure are represented as blue markers, with their sizes proportional to their respective resilience percentages. For example, the microgrid near the fire epicenter exhibits a resilience of 75%, reflecting moderate protection against fire impacts. The reservoir, located approximately 300 m south of the fire's origin, shows a resilience level of 60%, indicating a higher vulnerability due to its proximity and limited protective measures. In contrast, the evacuation center to the northeast demonstrates the highest resilience level at 90%, emphasizing its robust design and strategic location farther from high-risk zones.

Fig. 9 offers a high-resolution spatial assessment of how wildfire smoke and fire intensity jointly influence solar PV efficiency across the Pacific Palisades region. The heatmap illustrates the spatial distribution of PV efficiency reductions, with values declining from nearly 100% (light green) in unaffected zones to as low as 30% (dark green) in smoke-dense areas. Maximum efficiency degradation is concentrated near the fire origin at latitude 34.08° and longitude −118.62°, where smoke density is highest. The map integrates red contour lines denoting

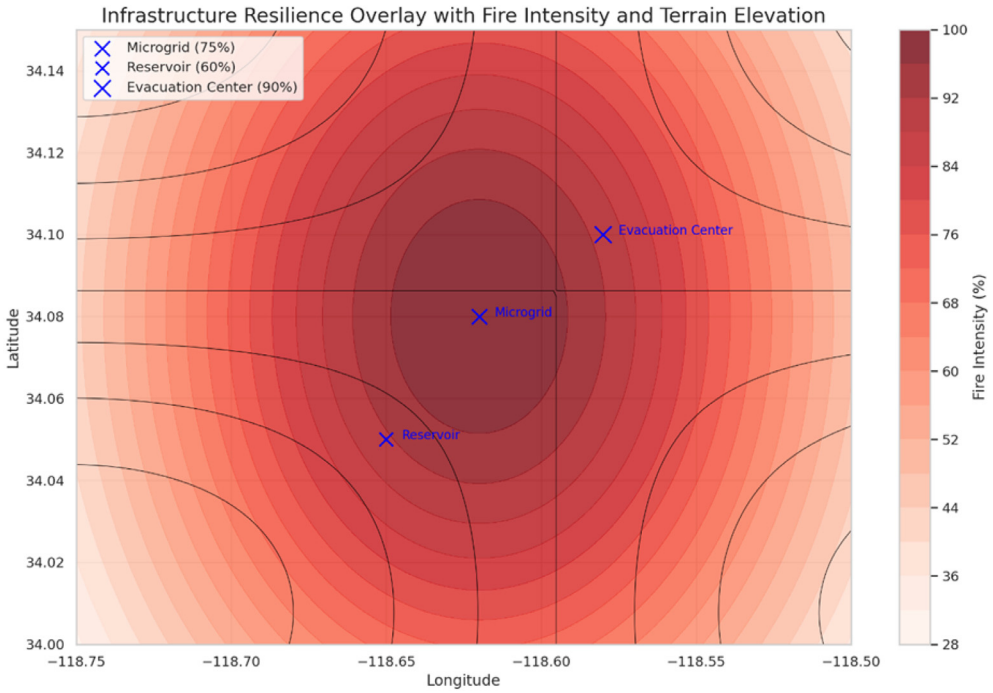


Fig. 8. Infrastructure resilience overlay with fire intensity and terrain elevation. (For interpretation of the references to color in this figure legend, the reader is referred to the web version of this article.)

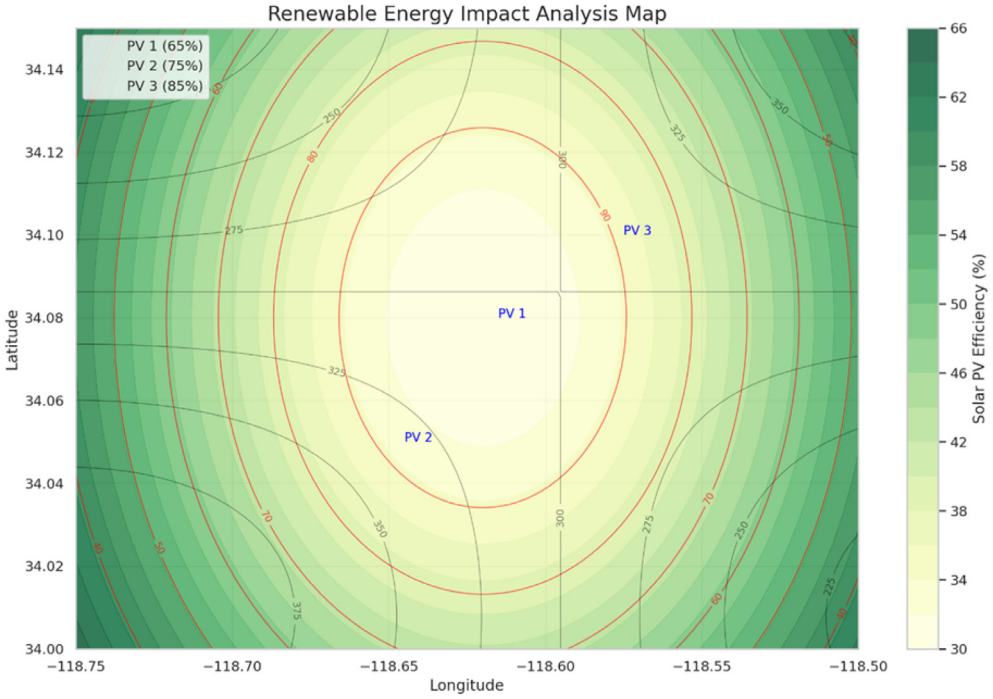


Fig. 9. Renewable energy impact analysis map. (For interpretation of the references to color in this figure legend, the reader is referred to the web version of this article.)

fire intensity — peaking centrally at 100% — and black contours representing terrain elevation, which ranges between 200 and 400 m. Elevated regions near the ignition zone intensify smoke accumulation and atmospheric turbidity, exacerbating solar attenuation and PV derating effects. To capture the compound influences on energy systems, critical PV installations are annotated using blue hollow circles, scaled in proportion to their post-impact efficiency. For instance, "PV 1", located within the high-density smoke plume, reports a reduced efficiency of 65%, while "PV 3", situated in a lower-risk area, maintains an efficiency of 85%. These spatial disparities emphasize the significance of terrain-induced airflow, smoke transport, and site vulnerability in determining local PV performance. Although the figure presents a representative spatial snapshot of smoke-induced PV efficiency degradation, the underlying framework is designed to accommodate the temporal variability that characterizes wildfire events. Smoke density

and particulate concentration often fluctuate on an hourly basis due to wind shifts, diurnal atmospheric cycles, and fire intensity changes. These factors can cause transient yet severe reductions in solar output, along with delayed recovery in PV efficiency. To address these dynamics, the model internally incorporates time-resolved data streams — such as real-time particulate measurements and updated weather forecasts — which inform adaptive battery dispatch, load curtailment, and reconfiguration strategies. The snapshot provided serves to illustrate one representative condition, while the full simulation process evolves over time to reflect changing operational constraints and environmental hazards. This integrated approach ensures that critical decisions remain responsive to both spatial heterogeneity and short-term temporal fluctuations during wildfire progression.

To highlight the practical value of the proposed method, a comparative perspective is provided against commonly employed strategies in wildfire-energy system coordination. Conventional models typically address either energy dispatch or wildfire progression in isolation, neglecting the coupled dynamics and feedbacks between these domains. By contrast, the presented framework jointly accounts for fire spread dynamics, uncertainty in renewable energy generation, and time-sensitive water resource management. Standard approaches often rely on static contingency plans or historical scenarios, which may prove inadequate during rapidly evolving fire conditions. In this context, the integration of dynamic fire propagation models, probabilistic resource forecasts, and critical load prioritization contributes to enhanced operational flexibility. Furthermore, while traditional planning methods emphasize average-case or long-term projections, the current formulation is designed to support real-time decision-making under emergency conditions. This includes explicit consideration of geographic variability, wind-driven fire behavior, and system interdependencies. Overall, the framework offers a more holistic and adaptive approach to infrastructure resilience in the face of compound wildfire hazards.

6. Conclusion

The ongoing wildfire crisis in Los Angeles, exemplified by the Palisades Fire, underscores the critical need for innovative frameworks that integrate energy, water, and wildfire management systems. This study introduced a comprehensive digital twin-based framework enhanced with DRO to address the multifaceted challenges posed by wildfires. By incorporating real-time data, advanced fire spread simulation, and coordinated resource allocation, the framework significantly improves the operational resilience of microgrids and critical infrastructure under extreme fire conditions.

Key findings demonstrate that coupling fire-aware modeling with adaptive energy and water coordination enables proactive response under uncertainty. The DRO-based formulation supports robust decision-making in the presence of stochastic renewable generation, variable water supply, and unpredictable fire dynamics. Nonetheless, the effectiveness of this framework is influenced by several practical constraints. The fidelity of wildfire simulation remains dependent on the resolution and accuracy of underlying environmental data, such as localized wind velocity, humidity, and vegetation distribution, which can vary across deployment regions. Moreover, the representation of energy and water systems is based on generalized component models, which may require site-specific calibration for operational deployment. Additionally, real-time execution of high-resolution fire simulations and DRO-based optimization may demand substantial computational resources, potentially limiting responsiveness in resource-constrained settings.

To enhance the generalizability and operational readiness of the framework, future work should consider integrating dense sensor networks to improve environmental observability, incorporating finer-grained infrastructure datasets, and optimizing algorithmic efficiency for real-time execution. The development of intuitive user interfaces to facilitate interactive use by emergency responders and system operators would also improve accessibility and adoption. Furthermore, expanding the model to accommodate compound disaster scenarios — such as concurrent wildfires and heatwaves — would broaden its applicability across multi-hazard contexts. The framework also holds promise for informing strategic investments in resilient infrastructure and shaping adaptive emergency response policies. Sustained interdisciplinary collaboration will be crucial to translating this research into practice. Partnerships among researchers, public agencies, utility operators, and technology providers can ensure the co-design of robust, context-aware solutions capable of responding to evolving climate risks. Continued efforts to validate, refine, and regionalize the framework will be essential for scaling its impact and ensuring long-term resilience in wildfire-prone communities. Overall, this study advances the integration of wildfire dynamics with infrastructure resilience planning, providing a foundation for scalable, adaptive, and data-driven decision support in the face of intensifying environmental challenges.

CRediT authorship contribution statement

Mohannad Alhazmi: Writing – original draft, Resources, Methodology, Funding acquisition. **Olivia Peijin Li:** Visualization, Software, Investigation. **Da Huo:** Validation, Supervision, Project administration. **Hanjin Zhang:** Writing – review & editing, Resources. **Zhaoyao Bao:** Visualization, Data curation.

Funding

This research was funded by Researchers Supporting Project grant number RSPD2025R635. And The APC was funded by Researchers Supporting Project (Project number: RSPD2025R635), King Saud University, Riyadh, Saudi Arabia.

Declaration of competing interest

The authors declare that they have no known competing financial interests or personal relationships that could have appeared to influence the work reported in this paper.

Acknowledgment

The authors would like to acknowledge the support provided by Ongoing Research Funding Program, (ORF-2025-635), King Saud University, Riyadh, Saudi Arabia.

All authors have read and approved the final version of the manuscript.

Data availability

Data will be made available on request.

References

Abdelmalak, M., Benidris, M., 2022. Enhancing power system operational resilience against wildfires. IEEE Trans. Ind. Appl. 58 (2), 1611–1621.

Analytica, O., 2025. California's Wildfire Response Receives Federal Aid. Emerald Expert Briefings, no. oxan-es.

Bassey, K.E., Opoku-Boateng, J., Antwi, B.O., Ntiakoh, A., 2024. Economic impact of digital twins on renewable energy investments. Eng. Sci. Technol. J. 5 (7), 2232–2247.

Boakye-Boateng, K., Ghorbani, A.A., Lashkari, A.H., 2025. Implementation of a trust-based framework for substation defense in the smart grid. Smart Cities 7 (1), 99–140. http://dx.doi.org/10.3390/smartcities7010005.

Brody-Heine, S., Zhang, J., Katurji, M., Pearce, H.G., Kittridge, M., 2023. Wind vector change and fire weather index in New Zealand as a modified metric in evaluating fire danger. Int. J. Wildland Fire 32 (6), 872–885.

Cao, W., Zhou, L., 2024. Resilient microgrid modeling in digital twin considering demand response and landscape design of renewable energy, sustainable energy. Technol. Assessments 64, 103628.

Cui, Y., Li, Y., Tang, H., Turowski, J.M., Yan, Y., Bazai, N.A., Wei, R., Li, L., 2024. A digital-twin platform for cryospheric disaster warning. Natl. Sci. Rev. 11 (10), nwae300.

Dobrinkova, N., 2024. Data accuracy challenges in wildland fire simulations. In: The International Conference on Environmental Protection and Disaster Risks. Springer, pp. 301–308.

Ermagun, A., Thompson, D., Vahedifard, F., Silver, R.C., 2025. Emergency managers' challenges with wildfires and related cascading hazards in california. J. Environ. Manag. 374, 124008.

Gao, Y., Ai, Q., 2024. Novel optimal dispatch method for multiple energy sources in regional integrated energy systems considering wind curtailment. CSEE J. Power Energy Syst. 10 (5), 2166–2173. http://dx.doi.org/10.17775/CSEEJPES.2021.01780.

Gao, Y., Ai, Q., He, X., Fan, S., 2023. Coordination for regional integrated energy system through target cascade optimization. Energy 276, 127606. http://dx.doi.org/10.1016/j.energy.2023.127606, 2023/08/01/.

Ghodrat, M., Shakeriaski, F., Fanaee, S.A., Simeoni, A., 2022. Software-based simulations of wildfire spread and wind-fire interaction. Fire 6 (1), 12.

Heluany, J.B., Gkioulos, V., 2024. A review on digital twins for power generation and distribution. Int. J. Inf. Secur. 23 (2), 1171–1195.

Jain, P., Castellanos-Acuna, D., Coogan, S.C., Abatzoglou, J.T., Flannigan, M.D., 2022. Observed increases in extreme fire weather driven by atmospheric humidity and temperature. Nat. Clim. Chang. 12 (1), 63–70.

Kadir, S.U., et al., 2021. Reinforcement learning based proactive control for transmission grid resilience to wildfire. arXiv preprint arXiv:2107.05756.

Li, P., Gu, C., Cheng, X., Li, J., Alhazmi, M., 2025a. Integrated energy-water systems for community-level flexibility: A hybrid deep Q-network and multi-objective optimization framework. Energy Rep. 13, 4813–4826. http://dx.doi.org/10.1016/j.egyr.2025.03.059, 2025/06/01/.

Li, P., Hu, Z., Shen, Y., Cheng, X., Alhazmi, M., 2025b. Short-term electricity load forecasting based on large language models and weighted external factor optimization. Sustain. Energy Technol. Assessments 82, 104449. http://dx.doi.org/10.1016/j.seta.2025.104449, 2025/10/01/.

Li, P., Shen, Y., Shang, Y., Alhazmi, M., 2025c. Innovative distribution network design using GAN-based distributionally robust optimization for DG planning. IET Gener. Transm. Distrib. 19 (1), e13350. http://dx.doi.org/10.1049/gtd2.13350.

Li, T.T., Zhao, A.P., Wang, Y., Alhazmi, M., 2025d. 'Hybrid energy storage for dairy farms: Enhancing energy efficiency and operational resilience'. J. Energy Storage 114, 115811. http://dx.doi.org/10.1016/j.est.2025.115811.

Price, S.J., Germino, M.J., 2022. Modeling of fire spread in sagebrush steppe using FARSITE: an approach to improving input data and simulation accuracy. Fire Ecol. 18 (1), 23.

Rahiminejad, A., Plotnek, J., Atallah, R., Dubois, M.-A., Malatrait, D., Ghafouri, M., Mohammadi, A., Debbabi, M., 2023. A resilience-based recovery scheme for smart grid restoration following cyberattacks to substations. Int. J. Electr. Power Energy Syst. 145, 108610. http://dx.doi.org/10.1016/j.ijepes.2022.108610, 2023/02/01/.

Scott, J.H., 2005. Standard Fire Behavior Fuel Models: A Comprehensive Set for Use with Rothermel's Surface Fire Spread Model. US Department of Agriculture, Forest Service, Rocky Mountain Research Station.

Solat, A., Gharehpetian, G.B., Naderi, M.S., Anvari-Moghaddam, A., 2024. On the control of microgrids against cyber-attacks: A review of methods and applications. Appl. Energy 353, 122037. http://dx.doi.org/10.1016/j.apenergy.2023.122037, 2024/01/01/.

Swann, D.E., Bellingham, P.J., Martin, P.H., 2024. Cyclone–fire interactions enhance fire extent and severity in a tropical montane pine forest. Ecosystems 1–18.

Umunnakwe, A., Huang, H., Oikonomou, K., Davis, K., 2021. Quantitative analysis of power systems resilience: Standardization, categorizations, and challenges. Renew. Sustain. Energy Rev. 149, 111252.

Wang, H., et al., 2025. Ultra-high-frequency harmony: mmwave radar and event camera orchestrate accurate drone landing. In: Proceedings of the 23rd ACM Conference on Embedded Networked Sensor Systems. pp. 15–29.

Xiao, J., Wang, L., Wan, Y., Bauer, P., Qin, Z., 2024. Distributed model predictive control based secondary control for power regulation in AC microgrids. IEEE Trans. Smart Grid http://dx.doi.org/10.1109/TSG.2024.3409154, 1–1.

Youvan, D.C., 2025. Facing the Flame: The Hidden Vulnerabilities of Los Angeles in the Era of Wildfire and Global Conflict.

Yu, D., He, Z., 2022. Digital twin-driven intelligence disaster prevention and mitigation for infrastructure: Advances. Challenges, Oppor. Nat. Hazards 112 (1), 1–36.

Zhao, P., Li, S., Cao, Z., Hu, P.J.-H., Zeng, D.D., Xie, D., Shen, Y., Li, J., Luo, T., 2024a. A social computing method for energy safety. J. Saf. Sci. Resil. 2024. http://dx.doi.org/10.1016/j.jnlssr.2023.12.001.

Zhao, A.P., Li, S., Li, Z., Wang, Z., Fei, X., Hu, Z., Alhazmi, M., Yan, X., Wu, C., Lu, S., Xiang, Y., Xie, D., 2024b. Electric vehicle charging planning: A complex systems perspective. IEEE Trans. Smart Grid http://dx.doi.org/10.1109/TSG.2024.3446859, 1–1.

Zhao, A.P., Zhang, Q., Alhazmi, M., Hu, P.J.-H., Zhang, S., Yan, X., 2024c. AI for science: Covert cyberattacks on energy storage systems. J. Energy Storage 99, 112835. http://dx.doi.org/10.1016/j.est.2024.112835, 2024/10/01/.

Zhao, A.P., et al., 2025. Hydrogen as the nexus of future sustainable transport and energy systems. Nat. Rev. Electr. Eng. 1–20.

Zhou, N., et al., 2025. Catua: Catalyzing urban air quality intelligence through mobile crowd-sensing. IEEE Trans. Mob. Comput..

DSPACE

https://dspace.org/

Can digital twin technology revolutionize wildfire management and energy resilience in Los Angeles?

Alhazmi, Mohannad; Li, Olivia Peijin; Huo, Da; Zhang, Hanjin; Bao, Zhaoyao

2025-12
Elsevier
https://doi.org/10.1016/j.egyr.2025.09.008
Alhazmi M, Li OP, Huo D, et al., (2025) Can digital twin technology revolutionize wildfire management and energy resilience in Los Angeles?. Energy Reports, Volume 14, December 2025, pp. 3118-3131

Downloaded from a DSpace repository. https://dspace.org/